**From Fluorite to Pyrochlore: Characterisation of Local and Average Structure of Neodymium Zirconate, $Nd_2Zr_2O_7$**

Julia L. Payne [a], Matthew G. Tucker [b] and Ivana Radosavljević Evans [a]
[a] *Department of Chemistry, Durham University, South Road, Durham. DH1 3LE, UK.*
[b] *ISIS Facility, Rutherford Appleton Laboratory, Didcot, Oxfordshire. OX11 0QX, UK.*

**Abstract**
The structural characterisation of $Nd_2Zr_2O_7$ prepared *via* a precursor route was performed using a combination of local and average structure probes (neutron total scattering, X-ray and neutron diffraction). We present the first total scattering and reverse Monte Carlo (RMC) modelling study of $Nd_2Zr_2O_7$, which provides compelling evidence for the adoption of a disordered fluorite-type structure by $Nd_2Zr_2O_7$ prepared by a low-temperature precursor route. Annealing the material at high temperatures leads to a transformation to a pyrochlore-type structure; however, Rietveld refinement using powder neutron diffraction data shows that the oxygen sublattice retains a degree of disorder.

## 1. Introduction

Mixed metal oxides with the general formula $A_2B_2O_7$ can adopt a number of structure types including pyrochlore and fluorite. Pyrochlores and fluorites display a variety of interesting properties, such as oxide ion conductivity, radiation stability, gas sensitivity, catalytic activity, superconductivity and giant magnetoresistivity [1-7]. In particular their potential as oxide ion conductors has led to the investigations of the fluorite-pyrochlore structural boundary, with the aim of correlating the degree of anion disorder to conductivity[2, 8]. The transformation of pyrochlore to fluorite may be induced thermally, on application of pressure and by chemical doping [2, 9, 10].

In the fluorite structure (space group *Fm*-3*m*), cations occupy the 4a site and anions occupy the 8c site. When a compound with composition $A_2B_2O_7$ adopts this structure, A and B cations are statistically disordered across the 4a sites, whilst oxygen and vacancies are statistically disordered across the 8c sites. When an ideal pyrochlore structure is adopted (space group *Fd*-3*m*), A and B cations and oxygen atoms are ordered, bringing about a doubling of the unit cell parameter with respect to fluorite. In an ideal pyrochlore, the A cation is eight coordinate, with the scalenohedral coordination environment comprising a puckered hexagon of anions plus two anions on the axial positions. The B cation coordination geometry is distorted octahedral. There are three relevant oxygen sites: 48*f* coordinated by two A and two B cations; 8*a* coordinated by four A cations, and the usually vacant oxygen site 8*b* is surrounded by four B cations. The geometry around each oxygen site is tetrahedral.

The relative stability of fluorite and pyrochlore structure types for a given composition is generally governed by cation radius ratio rules, $r_A/r_B$, with pyrochlore being stable in the region $r_A/r_B$ = 1.46-1.78 [1]. For many years, $Nd_2Zr_2O_7$ (with a cation radius ratio of 1.54) has been known to adopt the pyrochlore structure when synthesised *via* a conventional solid

state method. At 2300 °C $Nd_2Zr_2O_7$ undergoes a thermally induced pyrochlore-fluorite order-disorder transformation [9, 11]. Other compounds such as $Gd_2Zr_2O_7$ and $Sm_2Zr_2O_7$ also display similar transformations which have been attributed to the proximity of their $r_A/r_B$ ratios to the fluorite-pyrochlore stability boundary value of 1.46 [9].

The synthesis of $Nd_2Zr_2O_7$ by several precursor routes such as the sol-gel and citrate methods has also been reported [12-15]. However, there are conflicting descriptions of the $Nd_2Zr_2O_7$ product as a fluorite or pyrochlore structure. Lee *et al.* and Battacharya *et al*. report a fluorite structure when $Nd_2Zr_2O_7$ is synthesised at temperatures of 700 °C and 750 °C [12, 13]. Zhang assigns $Nd_2Zr_2O_7$ synthesised at 600 °C (for ten minutes) to the pyrochlore structure despite the PXRD data showing a poorly crystalline sample [15]. Rao reports the formation of $Nd_2Zr_2O_7$ at 500 °C but it is not clear whether this was assigned to the fluorite or pyrochlore structure [14]. This ambiguity in structure-type assignment primarily arises from the nature of the sample, with powder X-ray diffraction (PXRD) patterns showing poor crystallinity or broad peaks (as a result of small crystallite size). Due to the close structural relationship between fluorite and pyrochlore, the pyrochlore diffraction pattern consists of strong reflections (related to the fluorite substructure) and weaker pyrochlore superstructure reflections resulting from the ordering of cations and anions. When PXRD patterns show reflections with a large full-width at half maximum (FWHM), as in the case of $Nd_2Zr_2O_7$ products prepared by precursor methods, any relatively weak pyrochlore superstructure peaks can be difficult to detect. The majority of the existing structural characterisation of $Nd_2Zr_2O_7$ (prepared *via* precursor routes) has utilised powder X-ray diffraction. There are no neutron diffraction studies and there is only one example of use of a local structural probe (Fourier transform infra-red spectroscopy) [14].

The effect of the synthetic route on the structure adopted by the product has been demonstrated in a number of oxide materials. For example, for many years, cubic $ZrMo_2O_8$ could only be prepared via a precursor route, whilst solid state synthesis gave monoclinic $ZrMo_2O_8$ below 400$^o$C and trigonal $ZrMo_2O_8$ above this temperature [16]. However, recent work by Readman *et al.* has shown that cubic $ZrMo_2O_8$ can be synthesised from the oxides in seconds at high temperatures (1090-1130 $^o$C) [17]. $NaNbO_3$ also exhibits complex polymorphism related from the synthetic route used. A polar polymorph may be synthesised when a sol-gel method is used and the ilmenite polymorph of $NaNbO_3$ can only be prepared via hydrothermal synthesis [18, 19]; by adjusting the hydrothermal reaction conditions, a perovskite polymorph may be obtained [19]. $NaNbO_3$ also displays crystallite size related polymorphism [20].

The aim of our work was to determine the effect of the synthetic route on the structure of $Nd_2Zr_2O_7$ products obtained, using a range of average and local structure characterisation techniques including X-ray, neutron and electron diffraction, neutron total scattering and reverse Monte Carlo (RMC) modelling.

## 2. Experimental

### 2.1 Synthesis

Equimolar amounts of $Nd(NO_3)_3 \cdot 6H_2O$ and $ZrO(NO_3)_2 \cdot xH_2O$ were dissolved separately in 25 ml distilled water. The two solutions were mixed together and stirred thoroughly, before neutralising with $NH_4OH$ to yield a lilac gel. The resulting gel was stirred for several hours, aged overnight then stirred for a further two hours, before filtering under vacuum and washing with distilled water. The resulting solid was dried at 95 °C, yielding a precursor. The precursor was ground and fired at 800 °C for 16 hours (sample NZO800A). A second sample was annealed at 800 °C for 300 h, whilst a third sample was annealed for 1000 °C for 300 h (sample NZO1000).

### 2.2 Characterisation

PXRD data were collected on a Bruker D8 ADVANCE diffractometer, utilising $CuK\alpha_1$ radiation, equipped with a Ge monochromator, a VÅNTEC position sensitive detector and an Anton Parr HTK1200 high temperature stage. Typically, data were collected in the 10-70° 2θ range with a step size of 0.0170° and a counting time of 1 s per step, leading to a collection time of approximately one hour. Variable-temperature PXRD patterns were recorded in the temperature range 200-882 °C in 20 °C steps.

Powder neutron diffraction (PND) data were collected on GEM instrument at the ISIS facility. Approximately 8 g of sample were loaded into 8 mm vanadium cans. Data were collected in the 500-19900 μs time-of-flight range for a total of 140 μA h per sample for Rietveld-quality data, and 420 μA h for the total scattering data. The GEM diffractometer has a large number of detector elements covering a wide range of angles (1.2 ° to 171.4 °), and grouped into eight detector banks, giving a high resolution in both real and reciprocal space. The design and further technical details of the GEM detector arrays have been described by Hannon. [21]

Rietveld refinements were carried out using the TOPAS Academic software [22]. Neutron total scattering data were normalised onto an absolute scale using Gudrun [23]. This involves using data from a number of additional calibration runs to remove the background signal, take account of the neutron flux variation with wavelength and correct for absorption and multiple scattering. Following this process, the pair distribution function was obtained *via* a sine Fourier transform of the normalised diffraction data. RMCProfile was used for reverse Monte Carlo (RMC) modelling of the pair distribution function (PDF) data [24]. An $11 \times 11 \times 11$ fluorite supercell containing at total of 15972 atoms (2662 Nd, 2662 Zr, 9317 O and 1331 null scattering atoms as vacancies) and a $6 \times 6 \times 6$ pyrochlore supercell containing a total of 19008 atoms (3456 Nd, 3456 Zr, 10368 O (48*f* site) and 1728 O (8*a* site)) were used as the starting configurations for RMC modelling. The 'atom swap' function in RMCProfile was used to swap Nd atoms with Zr atoms and oxygen with oxygen vacancies in the fluorite model. Bond valence sum restraints were used to favour configurations with locally sensible coordination geometries and also to help guide the refinements during the initial stages [25]. RMC configurations were viewed using AtomEye [26].

Samples were prepared for electron diffraction by dispersing in a solvent and placing a drop on a holey carbon grid. A Jeol 2100F transmission electron microscope (TEM), operating at

200 keV and equipped with a Gatan Orius Camera CCD, was used to collect electron diffraction patterns.

## 3. Results and discussion

### 3.1 $Nd_2Zr_2O_7$ synthesised at 800 °C (NZO800A)

An *in-situ* variable temperature PXRD (VT-PXRD) experiment, using a heating rate of $10^o$/min, was carried out on the precursor to investigate the transformation to $Nd_2Zr_2O_7$. The precursor was essentially amorphous and the first Bragg peaks started appearing from 670 °C. Rietveld refinement confirmed the presence of a fluorite structure. No structural transformation (such as a transformation to a pyrochlore structure) was observed in the temperature range studied (up to 882 °C). This fluorite-type $Nd_2Zr_2O_7$ could also be annealed for over 300 h at 800 °C, without undergoing any structural transformation. The crystallite size of the samples during the annealing experiment, determined by Rietveld refinement of the laboratory XRD data, remains 10.5(1) nm. The fluorite structure is supported by refinements against three banks of GEM neutron diffraction data, with the overall $R_{wp}$ value of 2.171% (Figure 1). No pyrochlore peaks were observed in the diffraction pattern. However, due to the broad peaks in the powder diffraction patterns these data cannot be accepted as conclusive evidence of the fluorite structure.

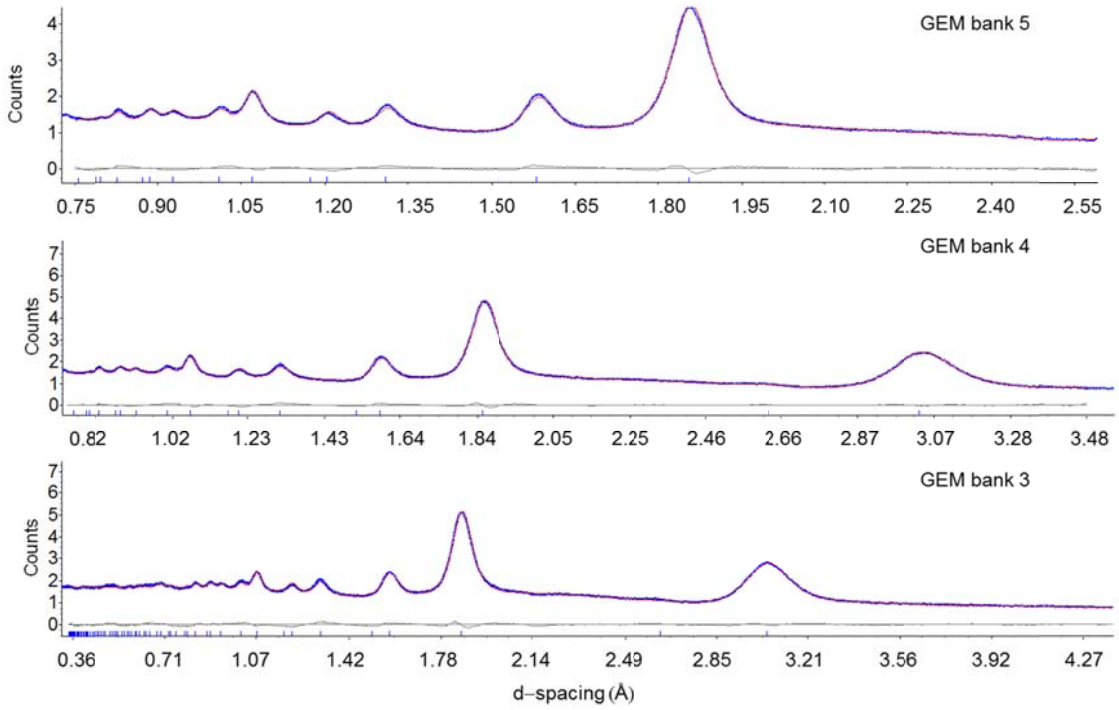


**Figure 1: Rietveld fit of $Nd_2Zr_2O_7$ (sample heated at $800^oC$, NZO800A) using a fluorite structural model and time-of-flight neutron diffraction data.**

Electron diffraction experiments were undertaken, but only ring patterns could be obtained due to a high degree of crystal agglomeration in the sample. The ring pattern (Figure 2), indexed to a ~5 Å face centred cubic unit cell, without any features suggesting a cell-doubling; this is consistent with the material adopting the fluorite structure.

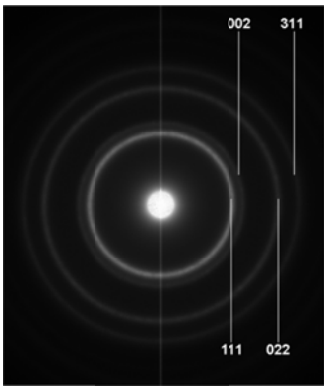


**Figure 2: Electron diffraction pattern of the NZO800A sample (heated at 800°C). The ring patterns obtained indexed to a ~5 Å face centred cubic unit cell, expected for the fluorite structure.**

To further investigate the structure, RMC refinements of the structure of NZO800A were carried out using both the pyrochlore and fluorite structures as starting configurations using PDF-quality data sets. Figure 3 shows the RMC fits to the total correlation function, T(r). T(r) is analogous to the pair distribution function (PDF), which represents the probability of finding an atom at a distance, r, from another atom. It is formally defined as:

$$T(r) = 4\pi r\rho_0\left[G(r) + \left(\sum_{i=1}^{n} c_i \overline{b_i}\right)^2\right]$$

where $\rho_0$ is the average number density, $\Sigma(c_i\overline{b}_i)^2$ is the total scattering cross section, and $G(r)$ is the total radial distribution function. The latter may be broken down into individual contributions from pairs of atoms, i.e. the partial radial distribution functions, $g_{ij}(r)$. Detailed mathematical descriptions of various correlation functions and quantities used to describe total scattering can be found in the review by Keen. [27]

Good fits were obtained when both the fluorite and pyrochlore starting configurations were used, as shown in Figure 3.

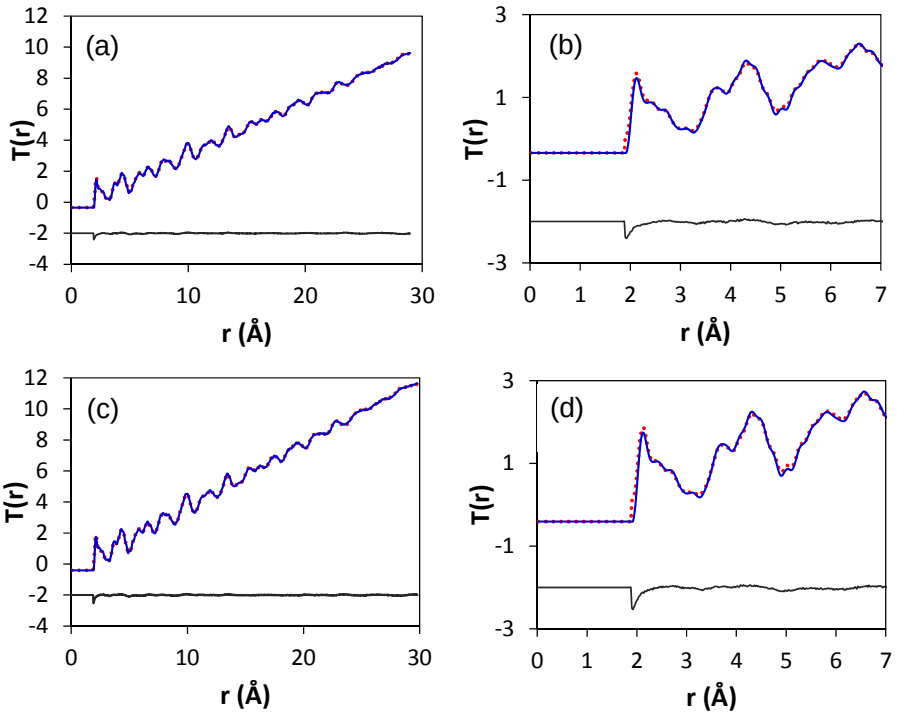


**Figure 3: Analysis of total scattering data collected on sample NZO800A (heated at 800°C): RMC fit to the T(r) using a fluorite starting configuration (Fig. 3 a-b) and a pyrochlore starting configuration (Fig. 3 c-d). Observed data shown as blue curves, calculated shown as red dots (for clarity and differentiation), and the difference curve shown in grey.**

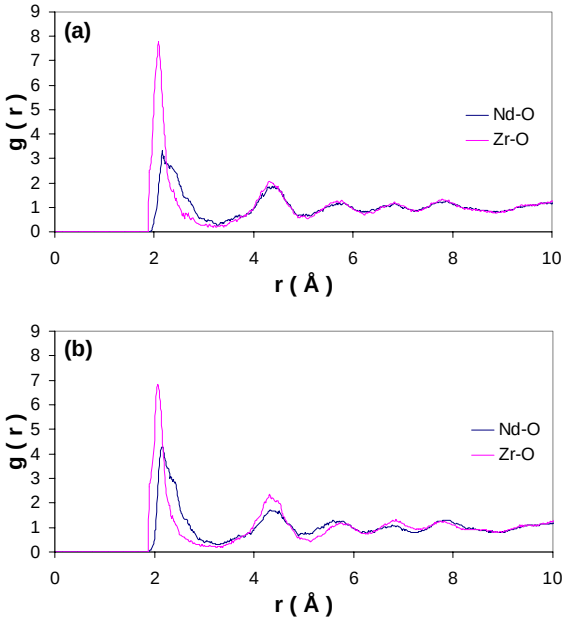


**Figure 4: Analysis of total scattering data collected on sample NZO800A (heated at 800°C): RMC bond length distributions from (a) the RMC configuration obtained from a fluorite starting model and (b) the RMC configuration obtained from a pyrochlore starting model.**

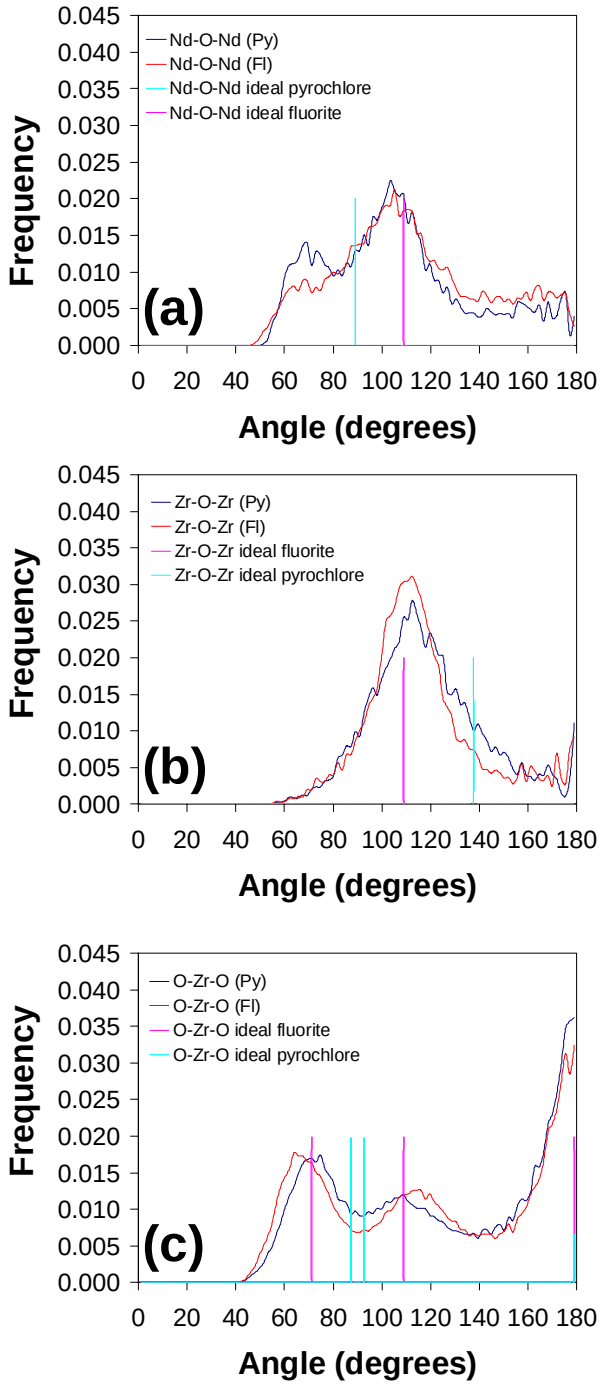


**Figure 5: Analysis of total scattering data collected on sample NZO800A (heated at 800°C): Comparison of bond angle distributions obtained from the RMC configuration obtained from a pyrochlore starting model and the RMC configuration obtained from a fluorite starting model. For comparison, the ideal fluorite (pink) and ideal pyrochlore (light blue) bond angles are shown as vertical lines. (a) Nd-O-Nd angles, (b) Zr-O-Zr angles and (c) O-Zr-O angles. Red curves are from the RMC configuration obtained from a fluorite starting model and dark blue curves are from the RMC configuration obtained from a pyrochlore starting model.**

The configurations obtained by RMC modelling can be best interpreted by analysing local geometries contained in the configurational models. Comparison of the bond length distributions shows very similar Nd-O and Zr-O bond lengths regardless of the initial structural model used, with the Nd-O bond length distribution centred around 2.18 Å and the Zr-O bond lengths centred around 2.08 Å, for the RMC configurations obtained from both the pyrochlore and fluorite starting models (Figure 4a and b). These are consistent with the relative ionic sizes of the two species, but cannot help us distinguish between the two structure types.

By contrast, the bond angles in the fluorite and pyrochlore structures provide sensitive means of differentiating between the two. The distributions of the key bond angles obtained by RMC modeling starting from the pyrochlore and fluorite initial configurations (dark blue and red curves, respectively) are shown in Figure 5, together with the lines representing the corresponding bond angles in the ideal pyrochlore and fluorite structures (light blue and pink vertical lines, respectively). Regardless of the starting model used, the main maximum of the Nd-O-Nd angle distribution is centred around the ideal fluorite value of 109° (pink vertical line in Figure 5a). The refined angles distribution maxima almost coincide, being at 104° and 105° for RMC configurations obtained from the pyrochlore and the fluorite starting models, respectively. In the ideal pyrochlore, the Zr-O-Zr angle is 138°, whilst in an ideal fluorite this angle is 109°. The Zr-O-Zr angle distributions obtained in RMC refinements from both starting models show clear centring around the ideal fluorite value of 109° (Figure 5b). The final bond angle parameter which allows differentiation between the pyrochlore and the fluorite structure types is the O-Zr-O angle. In the ideal pyrochlore structure, two values are expected around 90° (determined by the 48*f* oxygen *x* fractional coordinate) for the O-Zr-O angles (Figure 5c). However, following RMC refinements started from the pyrochlore structure, the distribution of this angle shows a clear distortion away from 90°, towards a bimodal distribution with the maxima centred at 73° and 109°, which are very close to the values of 71° and 109° typically observed for an ideal fluorite. When the RMC modelling starts from a fluorite model, these angles remain close to their initial values.

This analysis of trends obtained by RMC modelling demonstrates the clustering of the key structural parameters around the values characteristic of the fluorite structure, regardless of the starting model used. When RMC modelling was started from the fluorite model, the refined distributions of structural parameters remained close to the original ideal values. When RMC modelling was started from the pyrochlore structure, significant distortions were observed and the final parameter distributions end up centred around typical fluorite values.

Although the analysis of trends presented above is the most meaningful way to assess our RMC modelling results, we show the obtained fluorite configuration (Fig. 6a) alongside the ideal fluorite (Fig. 6b) and the ideal pyrochlore structure (Fig. 6c). In these figures, the original simulation boxes were collapsed back onto smaller cells, ($2\ a_F \times 2\ a_F \times 2\ a_F$) and a single pyrochlore cell (these correspond to the same metric). This graphically illustrates the disorder in both cation and oxygen sublattices, typical of the fluorite structure type. Neutron total scattering data hence provides compelling evidence that $Nd_2Zr_2O_7$ prepared *via* a precursor route is best described as having a fluorite structure.

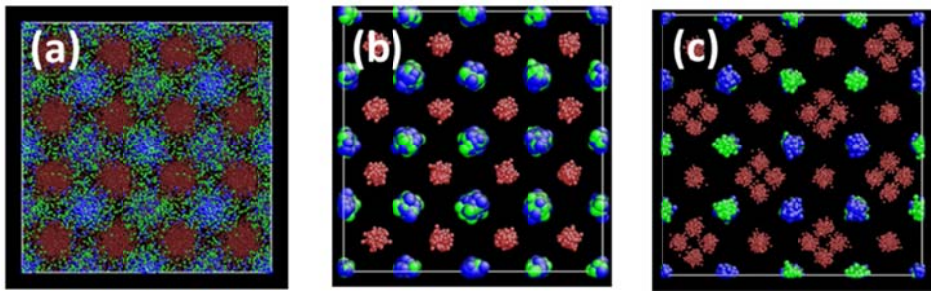


**Figure 6: Analysis of total scattering data collected on sample NZO800A (heated at 800°C): The final fluorite configuration obtained from RMCProfile refinements (a) compared to the ideal fluorite (b) and the ideal pyrochlore configuration (c). RMC configuration is condensed onto a 2 $a_F$ × 2 $a_F$ × 2 $a_F$ supercell, for comparison with the pyrochlore. Blue spheres are Nd atoms, green spheres Zr, red spheres O, grey spheres O' (for pyrochlore) and vacancy (for fluorite). $a_F$ ~5 Å (fluorite cell), $a_P$ ~10 Å (pyrochlore cell).**

### 3.2 $Nd_2Zr_2O_7$ annealed at 1000 °C (NZO1000)

Heating the fluorite-type $Nd_2Zr_2O_7$ sample at temperatures of 1000 °C or greater, leads to the adoption of the pyrochlore structure. This fluorite-pyrochlore transformation occurs at a temperature intermediate to those reported by Lee *et al.* (1100 °C) and Bhattacharya *et al.* (900 °C). PND data for structural analysis were collected on a sample annealed at 1000 °C for 300 hours, for which the laboratory XRD data suggest a crystallite size of 80.2(4) nm and clearly show the presence of the pyrochlore superstructure peaks.

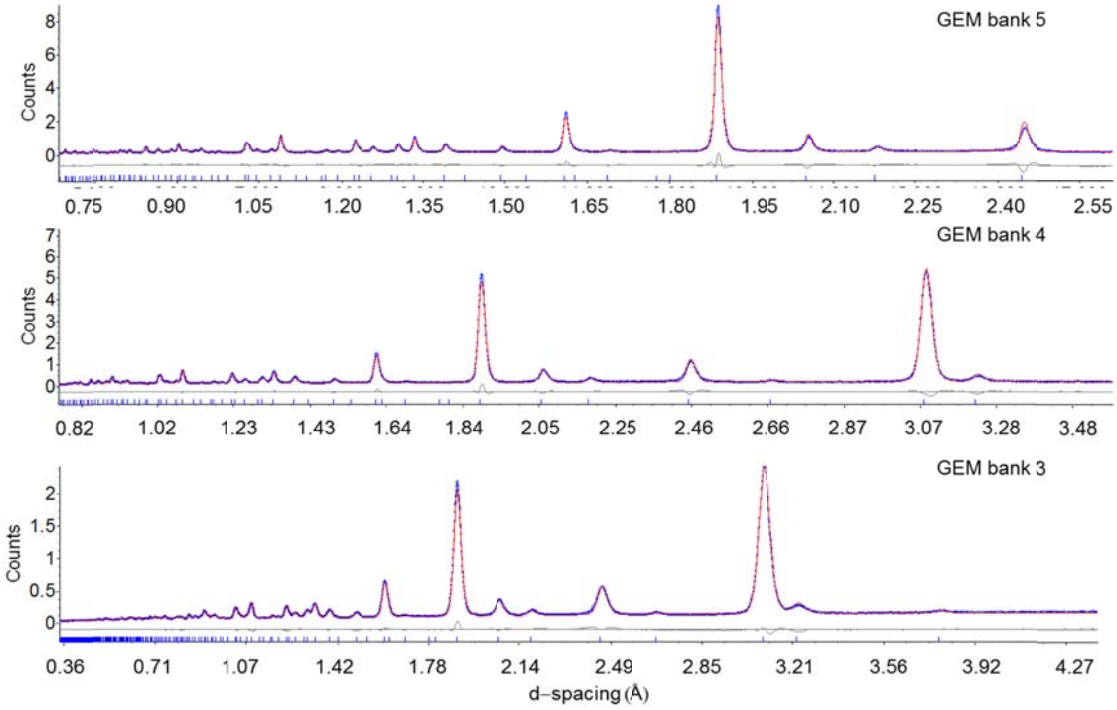


**Figure 7: Rietveld fit to the neutron data obtained for the NZO1000 sample (annealed at 1000°C) using a pyrochlore model with a disordered oxygen sublattice which includes occupation of the normally vacant O(3).**

The chemically similar $Nd_2Hf_2O_7$ was recently shown to be a disordered pyrochlore, with partial occupation of the usually vacant O(3) site [28]. Additionally, theoretical studies by Catlow and Wilde have shown that it is more energetically favourable to have defects on the O(1) (48*f*) site than the O(2) (8*a*) site [29]. This led us to test two models for the pyrochlore-type $Nd_2Zr_2O_7$ against our neutron data: Model 1, corresponding to an ideal pyrochlore structure with an ordered oxygen sublattice, and Model 2 with partial occupation of the O(3) sites (*i.e.* a disordered oxygen sublattice). Rietveld refinements were carried out using laboratory X-ray data and 3 banks of neutron data simultaneously. For both models, the zero point error, scale factor, absorption correction, 6 background parameters per bank, peak shape, cell parameter, 48*f x* coordinate of the O(1) site, one isotropic temperature factor per metal site and one equated isotropic temperature factor for all oxygen sites were refined. In addition, for Model 2, oxygen site occupancies were refined and a restraint was used for the occupancies to prevent deviations from the nominal $Nd_2Zr_2O_7$ stoichiometry. A summary of the models obtained from Rietveld refinement is given in Table 1. The best fit was obtained for the Model 2 with disordered oxygen sublattice and the fit is shown in Figure 7. The O(3) site was found to have an occupancy of 0.217(3), with the oxygen vacancies on the O(1) (48*f*) oxygen site; this reflects a small degree of fluorite-like character in this pyrochlore structure.

**Table 1: Structural models obtained from Rietveld refinements of pyrochlore-type $Nd_2Zr_2O_7$.**

| | **Model (1): without O(3)** | **Model (2): with O(3)** |
|---|---|---|
| *a* (Å) | 10.67699(5) | 10.67695(5) |
| $R_{wp}$ (%) | 6.035 | 5.488 |
| 48*f x* | 0.41119(5) | 0.41264(5) |
| Occupancy O(1) | 1 | 0.9659(8) |
| Occupancy O(2) | 1 | 0.991(3) |
| Occupancy O(3) | 0 | 0.217(3) |
| $B_{eq}$ oxygen ($Å^2$) | 1.30(1) | 1.16(1) |

It should be noted that a recent structural study of the $Ho_{2-x}Nd_xZr_2O_7$ system using powder neutron diffraction data also found a low level of occupation of the O(3) site for the pyrochlore-type $Nd_2Zr_2O_7$ prepared by conventional solid state synthesis, by heating the starting oxides 1450°C for 85 hours [30]. There is a difference between the obtained O(3) site fractional occupancy values for our $Nd_2Zr_2O_7$ sample and that reported by Clements *et al*. (where the O(3) site had an occupancy of 0.0061(5))[30]. However, this is not surprising, given different preparation methods and thermal histories of the two samples.

## 4. Conclusions

Local and average structure characterisation techniques (neutron total scattering and RMC modelling, X-ray, neutron and electron diffraction) have been employed in this study of $Nd_2Zr_2O_7$ prepared *via* a precursor method. The first total scattering study of $Nd_2Zr_2O_7$ is reported, and analysis of the distributions of key structural parameters obtained from RMC modelling clearly suggests that fluorite structure is adopted by the sample prepared at 800°C

from an amorphous precursor. This is also supported by X-ray, neutron and electron diffraction. Annealing this sample at 1000 °C results in a phase transition to a pyrochlore-type structure. However, Rietveld refinements using powder neutron diffraction data suggest that some disorder in the oxygen sublattice remains, imparting a small degree of fluorite-like character to the structure.

This work therefore emphasises an important general point, namely that the fluorite and the pyrochlore structures are better viewed as a continuously evolving structure type rather than as two distinct ones. In certain cases, the structural change will be accompanied by a significant change in physical properties. For example, in the $Y_2(Ti_{1-y}Zr_y)_2O_7$ series, a systematic substitution of the smaller $Ti^{4+}$ cation on the pyrochlore B-site by the larger $Zr^{4+}$ gradually drives the structure to a disordered fluorite-type, giving rise to increased oxide ion conductivity. [2]

**Acknowledgements**

We would like to thank STFC for beamtime, Budhika Mendis for collection of electron diffraction patterns, and Durham University for PhD studentship for JLP.

**References**

[1] M. A. Subramanian, G. Aravamundan, G.V.S. Rao, *Prog. Solid St. Chem* 15 (1983) 55-143.
[2] B.J. Wuensch, K.W. Eberman, C. Heremans, E.M. Ku, P. Onnerud, E.M.E. Yeo, S.M. Haile, J.K. Stalick, J.D. Jorgensen, *Solid State Ionics* 129 (2000) 111-133.
[3] K.E. Sickafus, L. Minervini, R.W. Grimes, J.A. Valdez, M. Ishimaru, F. Li, K.J. McClellan, T. Hartmann, *Science* 289 (2000) 748-751.
[4] G.S.V. Coles, S.E. Bond, G. Williams, *J. Mat. Chem.* 4 (1994) 23-27.
[5] Z.G. Zou, J.H. Ye, H. Arakawa, *Chem. Mater.* 13 (2001) 1765-1769.
[6] M. Hanawa, Y. Muraoka, T. Tayama, T. Sakakibara, J. Yamaura, Z. Hiroi, *Phys. Rev. Lett.* 87 (2001).
[7] Y. Shimakawa, Y. Kubo, T. Manako, *Nature* 379 (1996) 53-55.
[8] H. Yamamura, H. Nishino, K. Kakinuma, K. Nomura, *Solid State Ionics* 158 (2003) 359-365.
[9] D. Michel, M. Perez y Jorba, R. Collongues, *Mater. Res. Bull.* 9 (1974) 1457-1468.
[10] F.X. Zhang, B. Manoun, S.K. Saxena, *Mater. Lett.* 60 (2006) 2773-2776.
[11] E.J. Harvey, K.R. Whittle, G.R. Lumpkin, R.I. Smith, S.A.T. Redfern, *J. Solid State Chem.* 178 (2005) 800-810.
[12] A.K. Bhattacharya, A. Hartridge, K.K. Mallick, J.L. Woodhead, *J. Mater. Sci.* 29 (1994) 6076-6078.
[13] Y.H. Lee, H.S. Sheu, H.C.I. Kao, *Mater. Chem. Phys.* 124 (2010) 145-149.
[14] K.K. Rao, T. Banu, M. Vithal, G. Swamy, K.R. Kumar, *Mater. Lett.* 54 (2002) 205-210.
[15] A.Y. Zhang, M.K. Lu, Z.S. Yang, G.J. Zhou, Y.Y. Zhou, *Solid State Sciences* 10 (2008) 74-81.
[16] C. Lind, A.P. Wilkinson, Z.B. Hu, S. Short, J.D. Jorgensen, *Chem. Mater.* 10 (1998) 2335-2337.

[17] J.E. Readman, S.E. Lister, L. Peters, J. Wright, J.S.O. Evans, *J. Am.Chem. Soc.* 131 (2009) 17560-17562.
[18] K.E. Johnston, C.C. Tang, J.E. Parker, K.S. Knight, P. Lightfoot, S.E. Ashbrook, *J. Am. Chem. Soc.* 132 (2010) 8732-8746.
[19] D.R. Modeshia, R.J. Darton, S.E. Ashbrook, R.I. Walton, *Chem. Commun.* (2009) 68-70.
[20] Y. Shiratori, A. Magrez, M. Kato, K. Kasezawa, C. Pithan, R. Wasert, *Journal of Physical Chemistry C* 112 (2008) 9610-9616.
[21] A.C. Hannon, *Nuclear Instruments & Methods in Physics Research Section a-Accelerators Spectrometers Detectors and Associated Equipment* 551 (2005) 88-107.
[22] A.A. Coelho, J.S.O. Evans, I.R. Evans, A. Kern, S. Parsons, *Powder Diffraction* 26 (2011) S22.
[23] A.C. Hannon, W.S. Howells, A.K. Soper, *Institute of Physics Conference Series* (1990) 193-211.
[24] M.G. Tucker, D.A. Keen, M.T. Dove, A.L. Goodwin, Q. Hui, *J. Phys.: Condens. Matter* 19 (2007) 335218.
[25] S.T. Norberg, M.G. Tucker, S. Hull, *J. Appl. Cryst.* 42 (2009) 179-184.
[26] J. Li, *Modelling and Simulation in Materials Science and Engineering* 11 (2003) 173-177.
[27] D.A. Keen, *Journal of Applied Crystallography* 34 (2001) 172-177.
[28] R. Ubic, I. Abrahams, Y. Hu, *J. Am. Ceram. Soc.* 91 (2008) 235-239.
[29] P.J. Wilde, C.R.A. Catlow, *Solid State Ionics* 112 (1998) 173-183.
[30] R. Clements, J.R. Hester, B.J. Kennedy, C.D. Ling, A.P.J. Stampfl, *J. Solid State Chem.* 184 (2011) 2108-2113.